Testing General Relativity with the Shadow Size of Sgr A^{*}

Tim Johannsen, Avery E. Broderick, Philipp M. Plewa, Sotiris Chatzopoulos, Sheperd S. Doeleman, Frank Eisenhauer, Vincent L. Fish, Reinhard Genzel, Ortwin Gerhard, and Michael D. Johnson

Phys. Rev. Lett. **116**, 031101 — Published 19 January 2016

DOI: 10.1103/PhysRevLett.116.031101

Testing general relativity with the shadow size of Sgr A*

Tim Johannsen,[1,2] Avery E. Broderick,[1,2] Philipp M. Plewa,[3] Sotiris Chatzopoulos,[3] Sheperd S. Doeleman,[4,5] Frank Eisenhauer,[3] Vincent L. Fish,[4] Reinhard Genzel,[3,6] Ortwin Gerhard,[3] and Michael D. Johnson[5]

[1] *Perimeter Institute for Theoretical Physics, Waterloo, Ontario, N2L 2Y5, Canada*
[2] *Department of Physics and Astronomy, University of Waterloo, Waterloo, Ontario, N2L 3G1, Canada*
[3] *Max-Planck-Institut für extraterrestrische Physik, 85741 Garching, Germany*
[4] *MIT Haystack Observatory, Westford, MA 01886, USA*
[5] *Harvard-Smithsonian Center for Astrophysics, Cambridge, MA 02138, USA*
[6] *Physics and Astronomy Departments, University of California, 94720 Berkeley, USA*

In general relativity, the angular radius of the shadow of a black hole is primarily determined by its mass-to-distance ratio and depends only weakly on its spin and inclination. If general relativity is violated, however, the shadow size may also depend strongly on parametric deviations from the Kerr metric. Based on a reconstructed image of Sagittarius A* (Sgr A*) from a simulated one-day observing run of a seven-station Event Horizon Telescope (EHT) array, we employ a Markov chain Monte Carlo algorithm to demonstrate that such an observation can measure the angular radius of the shadow of Sgr A* with an uncertainty of ~ 1.5 μas (6%). We show that existing mass and distance measurements can be improved significantly when combined with upcoming EHT measurements of the shadow size and that tight constraints on potential deviations from the Kerr metric can be obtained.

PACS numbers: 04.50.Kd,04.70.-s

The mass M and distance D of Sgr A* have been measured using several techniques. Refs. [1–3] and Refs. [4, 5] inferred the mass and distance of Sgr A* from monitoring stars on orbits around Sgr A* and in the old Galactic nuclear star cluster, respectively. Combining the results of Refs. [2, 5] yields the measurements $M = (4.23 \pm 0.14) \times 10^6 M_\odot$, $D = 8.33 \pm 0.11$ kpc [5]. In addition, the distance of Sgr A* has been obtained from parallax and proper motion measurements of masers throughout the Milky Way by Ref. [6] finding $D = 8.34 \pm 0.16$ kpc. Sgr A* is also a prime target of the EHT, a global very-long baseline interferometer, which has already resolved structures on scales of only $8r_g$ with a three-station array [7], where $r_g \equiv GM/c^2$ is the gravitational radius.

According to the general-relativistic no-hair theorem, stationary, electrically neutral black holes in vacuum only depend on their masses M and spins J and are uniquely described by the Kerr metric. Mass and spin are the first two multipole moments of the Kerr metric, and all higher-order moments can be expressed by the relation $M_l + iS_l = M(ia)^l$, where M_l and S_l are the mass and current multipole moments, respectively, and $a \equiv J/M$ is the spin parameter (see, e.g., [8]). However, general relativity remains practically untested in the strong-field regime found around compact objects, and a final proof of the Kerr nature of black holes is still lacking [9].

The no-hair theorem can be tested in a model-independent manner using parametrically deformed Kerr-like spacetimes that depend on one or more free parameters in addition to mass and spin. Observations may then be used to measure the deviations. If none are detected, the compact object is consistent with a Kerr black hole. If, however, nonzero deviations are measured, there are two possible interpretations: 1. general relativity holds but the object is some exotica instead of a black hole, 2. the no-hair theorem is falsified.

Such Kerr-like spacetimes encompass many theories of gravity at once and the underlying action is usually unknown. Here, we employ the Kerr-like metric of Ref. [10] with the nonzero (dimensionless) deviation parameters α_{13} and β. This metric can be mapped to known black hole solutions of alternative gravity theories for certain choices of these (and other) parameters and reduces to the Kerr metric if all deviations vanish [10, 11].

A key objective of the EHT is to produce the first direct image of a black hole [34]. These typically reveal a dark region at the center, the so-called shadow, which is surrounded by a bright and narrow ring-like structure embedded within a typically complex image [35]. For a Kerr black hole at a distance D, the angular radius R of its shadow is $R \approx 5r_g/D$. The shape of this shadow is exactly circular for a Schwarzschild black hole and nearly circular for a Kerr black hole unless its spin is very large and the inclination is high [36]. However, if the no-hair theorem is violated, the shape of the shadow can become asymmetric [36] and its size can vary [37, 38].

If Sgr A* is indeed a Kerr black hole, then its angular radius measured by upcoming EHT observations has to coincide with the angular radius inferred from existing measurements of the mass and distance of Sgr A* [39]. For nonzero values of the parameters α_{13} and β in the metric of Ref. [10], the shadow size either increases or decreases drastically, retaining a nearly circular shape as long as $a \lesssim 0.9 r_g$ [37, 38], while dynamical measurements of the mass and distance would be unaffected. Thus, the combination of both techniques allows us to constrain the deviation parameters α_{13} and β. In addition, measurements of the ratio M/D by the EHT can improve upon

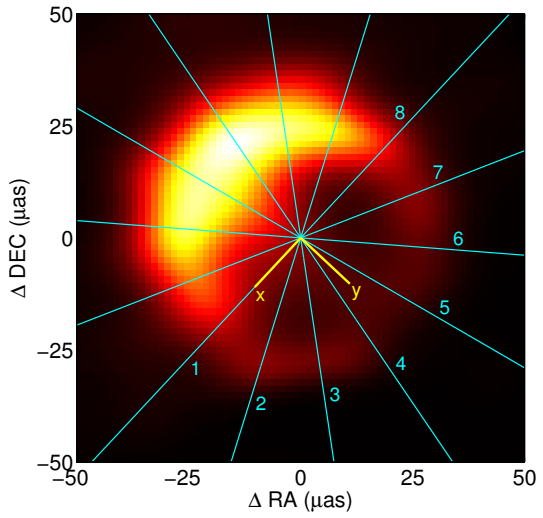

FIG. 1. The top panel shows a reconstructed image of Sgr A* for an EHT observation at 230 GHz with a seven-station array taken from Ref. [41]. The image shows seven chords for which we determined respective angular radii from Gaussian fits of the intensity profile along the chord sections labeled "1",...,"8." The bottom panel shows the resulting distributions of the angular radius R of the shadow and the offset (x, y) of the corresponding image center relative to the center of the chords using a Markov chain Monte Carlo sampling of a small region around the center of the chords.

the existing mass and distance measurements [40].

Here, we investigate the prospects of measuring the angular radius R of the shadow of Sgr A* with the EHT at 230 GHz assuming a circular shadow. We use a reconstructed image of Sgr A* based on a simulated image of a radiatively-inefficient accretion flow [41]. The deblurring algorithm of Ref. [41] corrects the distortions of the simulated visibilities by interstellar scattering so that the resolution of the image is predominantly determined by the instrumental beam.

The top panel of Fig. 1 shows the reconstructed image of Ref. [41] using the data of a simulated one-day observing run with a seven-station EHT array assuming realistic measurement conditions but neglecting small-scale variability in the image. The large-scale features within the image are asymmetric due to the relativistic motion of the emitting plasma and opacity. Nevertheless, over at least half of the image the photon ring is clearly visible. To estimate its size we first obtain a set of mean radii $\bar{r}_j$ from Gaussian fits of the specific intensity along the chord sections $j = 1, \ldots, 8$ shown in Fig. 1 [11].

The chosen center of the chords most likely does not coincide exactly with the true image center which will be shifted by an offset $\mathbf{x} = (x, y)$ relative to the center of the chords (see Fig. 1). A measured angular radius vector $\bar{\mathbf{r}}_\mathbf{j} = (\bar{r}_j \cos\theta, \bar{r}_j \sin\theta)$ is then related to the angular radius vector of the shadow $\mathbf{R}$ and the offset $\mathbf{x}$ by the identity $\bar{\mathbf{r}}_\mathbf{j} = \mathbf{R} - \mathbf{x}$, i.e., $\bar{r}_j = -(x\cos\theta + y\sin\theta) + \sqrt{(x\cos\theta + y\sin\theta)^2 + R^2 - (x^2 + y^2)}$.

From the set of angular radii $\bar{r}_j$ we then obtain estimates of the angular shadow radius R and the offsets x and y using a Markov chain Monte Carlo sampling of a small region around the center of the chords. We find that each of the resulting distributions of the angular shadow radius R and the offsets x and y is approximately Gaussian and that the angular radius R is correlated with the offset y, while both the angular radius R and the offset y appear to be uncorrelated with the offset x (see Fig. 2). Thus, we infer $x = (-0.3 \pm 1.1)$ μas, $y = (1.3 \pm 2.2)$ μas, and $R = (26.4 \pm 1.5)$ μas, which corresponds to a distance $\sim 0.16 r_g$ and a $\sim 6\%$ uncertainty of the angular radius. This is comparable to the one of Ref. [39], who used a pattern matching technique.

Although we find no significant values of the offsets x and y, we repeated this process several times by slightly shifting the center of the chords and obtained a similar result in each case. Our estimate of the angular radius is consistent with the actual angular radius of the shadow $R \approx 27.6$ μas at the 1σ level corresponding to the values of the mass $M = 4.3 \times 10^6 M_\odot$, distance $D = 8$ kpc, and spin $a = 0$ used in the simulated image shown in Fig. 1. Because the radius estimate would be exact for a true image [42], our method seems to have no significant bias.

We combine the above simulated EHT measurement of the angular shadow radius of Sgr A* with existing measurements of its mass and distance which we use as a prior $P_{\rm prior}(M, D)$. We assume a Gaussian distribution $P_{\rm EHT}({\rm data}|M, D, a, \vartheta, \alpha_{13}, \beta)$ of the angular radius with an uncertainty $\sigma = 1.5$ μas and a mean corresponding to the maximum of the distribution $P_{\rm prior}(M, D)$ of the combined measurements of Refs. [2, 5, 6] assuming a Kerr black hole with spin $a = 0.5 r_g$ and inclination $\vartheta = 60°$. For given values of the mass, distance, and deviation parameters, we calculate the angular radius of the shadow as described in Refs. [37, 38]. Because the shadow size depends only weakly on the spin and inclination we marginalize over the spin and inclination using Eq. (42) of Ref. [38] in the case of a Kerr black hole and a fine grid of points (a, ϑ) in the case of non-Kerr black holes. Last, we use Bayes' theorem to express the likelihood of the mass, distance, and deviation parameters given the data as $P(M, D, \alpha_{13}, \beta|{\rm data}) = C\ P_{\rm EHT}({\rm data}|M, D, \alpha_{13}, \beta) P_{\rm prior}(M, D)$, where C is a normalization constant. For simplicity, we also consider the modifications of the shadow size introduced by the parameters α_{13} and β separately.

Joint constraints from various measurements of M and D are combined in Fig. 2; where indicated we presume forthcoming 30m-class telescope stellar dynamics observations will make roughly 0.1% measurements of M and D [43]. Here, we assume that all EHT measurements are independent and identical allowing us to reduce their uncertainty by a factor of $\sqrt{N}$. In practice, one EHT

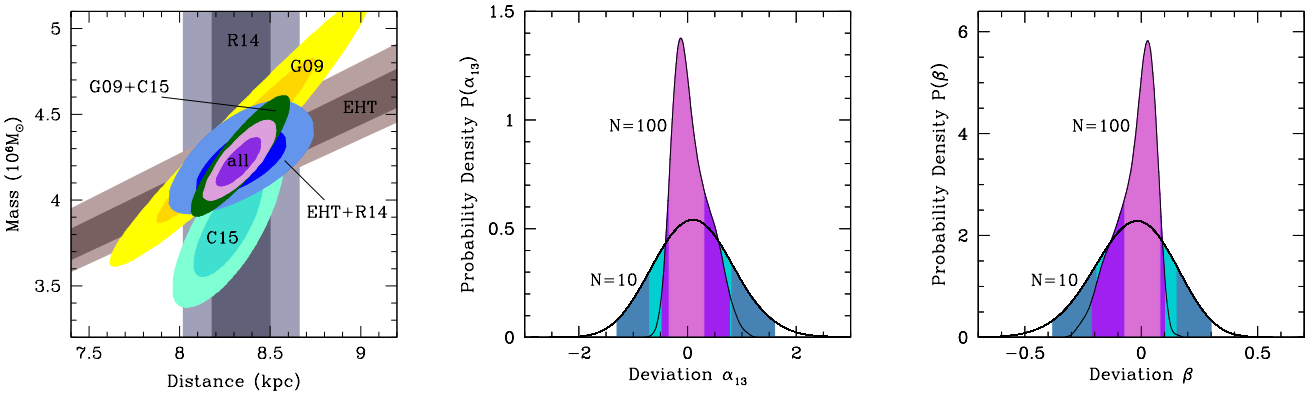

FIG. 2. Left panel: 1σ and 2σ confidence contours of the probability density of the mass and distance of Sgr A* for existing measurements (S-stars, "G09" [2]; masers, "R14" [6]; star cluster, "C15" [5]), a simulated measurement of the shadow size of Sgr A* for $N = 10$ observations with a seven-station EHT array ("EHT"), and several combinations thereof. The simulated EHT measurement improves the other constraints on the mass and distance significantly. Center and right panels: Simulated 1σ and 2σ confidence contours of the probability density of the deviation parameters α_{13} and β, respectively, corresponding to $N = 10$ and $N = 100$ EHT observations, each marginalized over the mass and distance using the combination of all data sets ("all") in the $N = 10$ case and of simulated stellar-orbit observations from a 30m-class telescope [43] in the $N = 100$ case.

measurement likely corresponds to an average of several observations due to small-scale variations in the image which we neglect here.

We find that the EHT alone can measure the mass-distance ratio (in units of $10^6 M_\odot$/kpc) $M/R = 0.505^{+0.013+0.029}_{-0.011-0.020}$ for $N = 10$ observations and $M/R = 0.502^{+0.010+0.026}_{-0.005-0.007}$ for $N = 100$ observations, respectively. Table I lists constraints on the mass and distance corresponding to various combinations of the EHT measurements for 10 observations with existing data showing significant improvements, facilitated by different correlations of mass and distance (stellar orbits: roughly $M \sim D^2$ [1, 2]; EHT: $M \sim D$ [40]). In particular, combining the EHT result with the parallax measurement by Ref. [6] is comparable to the mass and distance measurements from stellar orbits including the combined result of Refs. [2, 5]. Combining all data sets, we obtain the constraints on the deviation parameters $\alpha_{13} = 0.1^{+0.7+1.5}_{-0.8-1.4}$, $\beta = -0.02^{+0.17+0.32}_{-0.17-0.36}$ in the $N = 10$ case, while, in the $N = 100$ case, we find $\alpha_{13} = -0.13^{+0.43+0.90}_{-0.21-0.34}$, $\beta = 0.03^{+0.05+0.07}_{-0.10-0.24}$; the uncertainties of the mass and distance remain at the $\sim 0.1\%$ level. Here, all results are quoted with 1σ and 2σ error bars, respectively. Our results would also imply constraints on the couplings of specific gravity theories, summarized in Table II, and could improve upon spin measurements by other methods [11].

We have assumed that the image of Sgr A* is constant, but two effects will cause the apparent structure of the source to be variable. First, the accretion flow will be intrinsically variable on characteristic timescales on the order of minutes to tens of minutes. These rapid changes will complicate image reconstructions from EHT data, which conventionally assume a static source over each observing epoch. Second, interstellar scattering will blur the source image, which reduces the sensitivity of the long baselines of the EHT but is largely invertible. Since we fit the specific intensity along the chords with Gaussians, our method is insensitive to remaining uncertainties in the interstellar scattering law. Interstellar scattering will also introduce refractive substructure into the apparent

Data	Mass ($10^6 M_\odot$)	Distance (kpc)
EHT+G09	$4.16^{+0.18+0.38}_{-0.16-0.31}$	$8.18^{+0.19+0.39}_{-0.19-0.37}$
EHT+R14	$4.22^{+0.13+0.28}_{-0.13-0.24}$	$8.34^{+0.16+0.32}_{-0.15-0.31}$
EHT+C15	$4.17^{+0.11+0.22}_{-0.11-0.21}$	$8.38^{+0.11+0.21}_{-0.11-0.21}$
All	$4.22^{+0.09+0.20}_{-0.09-0.17}$	$8.33^{+0.08+0.17}_{-0.08-0.15}$

TABLE I. Simulated mass and distance measurements using existing data (G09 [2]; R14 [6]; C15 [5]) as priors.

Theory	Constraints ($N = 10$)	Constraints ($N = 100$)
RS2	$\beta_{\rm tidal} = -0.02^{+0.17+0.32}_{-0.17-0.36}$	$\beta_{\rm tidal} = 0.03^{+0.05+0.07}_{-0.10-0.24}$
MOG	$\alpha = -0.02^{+0.13+0.22}_{-0.13-0.24}$	$\alpha = 0.03^{+0.05+0.06}_{-0.08-0.17}$
EdGB	$\zeta_{\rm EdGB} \approx 0^{+0.1+0.2}_{-0.1-0.3}$	$\zeta_{\rm EdGB} \approx 0.022^{+0.035+0.057}_{-0.072-0.150}$

TABLE II. 1σ and 2σ constraints on the parameters of black holes in Randall-Sundrum type braneword gravity (RS2 [44]), Modified Gravity (MOG [45]), and Einstein-dilaton-Gauss-Bonnet gravity (EdGB [46]) implied by our simulation.

image which can cause image distortions that will vary stochastically from epoch to epoch [41, 47].

While intrinsic source variability and refractive substructure are very different processes, their primary mitigation strategy is to repeat observations over many epochs. It will be possible to image the quiescent accretion flow by imaging data obtained over the course of several nights, over which time the source variability will average out [48]. Likewise, the effects of different realizations of refractive substructure on different observing days will average out.

Our estimate will also be affected moderately by systematic uncertainties in the EHT calibration and the accretion flow model in the image reconstruction. In order to properly account for the calibration uncertainties in our estimate, perhaps the best approach is to reconstruct images using not only the best-calibrated data but also a number of datasets that are intentionally miscalibrated by a small amount. While the detailed structure of the accretion flow of Sgr A* is unknown and could have, e.g., other (vertical or horizontal) configurations of the plasma density and magnetic fields, as well as outflows, we expect that these uncertainties only play a subdominant role in our simulation as long as a (nearly circular) shadow is clearly visible in the image, because the size and shape of the shadow are almost entirely determined by the underlying spacetime alone [11].

Before a 30m-class optical telescope will be available, the uncertainties of mass and distance measurements based on stellar orbits will be further reduced by continued monitoring and the expected improvement in astrometry with the second-generation instrument GRAVITY for the Very Large Telescope Interferometer [49].

T.J. is supported in part by Perimeter Institute for Theoretical Physics. A.E.B. receives financial support from Perimeter Institute for Theoretical Physics and the Natural Sciences and Engineering Research Council of Canada through a Discovery Grant. Research at Perimeter Institute is supported by the Government of Canada through Industry Canada and by the Province of Ontario through the Ministry of Research and Innovation. The Event Horizon Telescope is supported by grants from the National Science Foundation, from the Gordon and Betty Moore Foundation (#GBMF-3561), from the Smithsonian Institution, and with generous equipment donations from Xilinx Inc. and HGST Inc.

[1] A.M. Ghez, S. Salim, N.N. Weinberg, et al., Astrophys. J. **689**, 1044 (2008).
[2] S. Gillessen, F. Eisenhauer, S. Trippe, et al., Astrophys. J. **692**, 1075 (2009).
[3] L. Meyer, A.M. Ghez, R. Schödel, S. Yelda, A. Boehle, J.R. Lu, T. Do, M.R. Morris, E.E. Becklin, and K. Matthews, Science **338**, 6103 (2012).
[4] T. Do, G.D. Martinez, S. Yelda, A.M. Ghez, J. Bullock, M. Kaplinghat, J.R. Lu, A.G.H. Peter, and K. Phifer, Astrophys. J. **779**, L6 (2013).
[5] S. Chatzopoulos, T.K. Fritz, O. Gerhard, S. Gillessen, C. Wegg, R. Genzel, and O. Pfuhl, MNRAS **447**, 948 (2015).
[6] M.J. Reid, K.M. Menten, A. Brunthaler, et al., Astrophys. J. **783**, 130 (2014).
[7] S.S. Doeleman, J. Weintroub, A.E.E. Rogers, et al., Nature **455**, 78 (2008).
[8] M. Heusler, Black Hole Uniqueness Theorems (Cambridge University Press, Cambridge, England, 1996).
[9] D. Psaltis, Living Rev. Rel. **11**, 9 (2008).
[10] T. Johannsen, Phys. Rev. D **88**, 044002 (2013).
[11] See Supplementary Material [url], which includes Refs. [12–33].
[12] K. Glampedakis and S. Babak, Class. Quantum Grav. **23** 4167 (2006).
[13] S.J. Vigeland and S.A. Hughes, Phys. Rev. D **81**, 024030 (2010).
[14] S.J. Vigeland, N. Yunes, and L.C. Stein, Phys. Rev. D **83**, 104027 (2011).
[15] T. Johannsen and D. Psaltis, Phys. Rev. D **83**, 124015 (2011).
[16] R.M. Wald, General Relativity (University of Chicago Press, Chicago, 1984).
[17] T. Johannsen, Phys. Rev. D **87** 124010 (2013).
[18] C.W. Misner, K.S. Thorne, and J.A. Wheeler, Gravitation (W. H. Freeman and Company, New York, 1973).
[19] C.M. Will, Living Rev. Rel. **17** 4 (2014).
[20] C.M. Will, Theory and Experiment in Gravitational Physics (Cambridge University Press, Cambridge, 1993).
[21] K. Yagi, N. Yunes, and T. Tanaka, Phys. Rev. D **86** 044037 (2012).
[22] T. Johannsen, Class. Quantum Grav., in preparation.
[23] A.E. Broderick, T. Johannsen, A. Loeb, and D. Psaltis, Astrophys. J. **784**, 7 (2014).
[24] J.R. Gair, M. Vallisneri, S.L. Larson, and J.G. Baker, Living Rev. Rel. **16** 7 (2013).
[25] B. Aschenbach, N. Grosso, D. Porquet, and P. Predehl, Astron. Astrophys. **417** 71 (2004); S. Trippe, T. Paumard, T. Ott, S. Gillessen, F. Eisenhauer, F. Martins, and R. Genzel, MNRAS **375** 764 (2007).
[26] K. Liu, N. Wex, M. Kramer, J.M. Cordes, and T.J.W. Lazio 2012, Astrophys. J. **747** 1
[27] T. Johannsen, Phys. Rev. D **90** 064002 (2014); N. Lin, Z. Li, J. Arthur, R. Asquith, and C. Bambi, JCAP **09** 038 (2015).
[28] V.L. Fish, S.S. Doeleman, C. Beaudoin, et al., Astrophys. J. **727** 36 (2011).
[29] R. Narayan, R. Mahadevan, J E. Grindlay, R.G. Popham, and C.F. Gammie, Astrophys. J. **492**, 554 (1998); R.D. Blandford and M.C. Begelman, MNRAS **303**, L1 (1999); H. Falcke and P.L. Biermann, Astron. Astrophys. **342**, 49 (1999); F. Özel, D. Psaltis, and R. Narayan, Astrophys. J. **541**, 234 (2000); F. Yuan, E. Quataert, and R. Narayan, Astrophys. J. **598**, 301 (2003).
[30] M. Mościbrodzka, C.F. Gammie, J.C. Dolence, H. Shiokawa, and P.K. Leung, Astrophys. J. **706** 497 (2009); J. Dexter, E. Agol, and P.C. Fragile, Astrophys. J. **703** L142 (2009); R. Shcherbakov and R. Penna, in The Galactic Center: A Window to the Nuclear Activity of Disk Galaxies, ed. M. Morris et al. (San Francisco, CA:

ASP, 2011), 372; C.-K. Chan, D. Psaltis, F. Özel, R. Narayan, and A. Sadowski, Astrophys. J. **799** 1 (2015).
[31] D. Psaltis and T. Johannsen, J. Phys. Conf. Ser. **283** 012030 (2011).
[32] A.E. Broderick, V.L. Fish, S.S. Doeleman, and A. Loeb, Astrophys. J. **697** 45 (2009); ibid., Astrophys. J. **735** 110 (2011); A.E. Broderick, V.L. Fish, M.D. Johnson, et. al., submitted to Astrophys. J.
[33] C.M. Will, Astrophys. J. **674** L25 (2008).
[34] S.S. Doeleman, E. Agol, D. Backer, et al., *Astro2010: The Astronomy and Astrophysics Decadal Survey*, Science White Papers **68** (2009).
[35] J.M. Bardeen in *Black Holes*, Gordon and Breach (1973); J.-P. Luminet, Astron. Astrophys. **75**, 228 (1979); H. Falcke, F. Melia, and E. Agol, Astrophys. J. **528**, L13 (2000); R. Takahashi, Astrophys. J. **611**, 996 (2004).
[36] T. Johannsen and D. Psaltis, Astrophys. J. **718**, 446 (2010).
[37] L. Amarilla and E.F. Eiroa, Phys. Rev. D **85**, 064019 (2012).
[38] T. Johannsen, Astrophys. J. **777**, 170 (2013).
[39] D. Psaltis, F. Özel, C.-K. Chan, and D.P. Marrone, Astrophys. J. **814** 115 (2015).
[40] T. Johannsen, D. Psaltis, S. Gillessen, D.P. Marrone, F. Özel, S.S Doeleman, and V.L. Fish, Astrophys. J. **985**, 30 (2012).
[41] V.L. Fish, M.D. Johnson, R.-S. Lu, et al., Astrophys. J. **795**, 134 (2014).
[42] The specific intensity peaks at the shadow corresponding to the longest optical photon path in the accretion flow.
[43] N.N. Weinberg, M. Milosavljević, and A.M. Ghez, Astrophys. J. **622**, 878 (2005).
[44] A.N. Aliev and A.E. Gümrükçüoğlu, Phys. Rev. D **71** 104027 (2005).
[45] J.W. Moffat, Europ. Phys. J. C **75** 175 (2015).
[46] D. Ayzenberg and N. Yunes, Phys. Rev. D **90** 044066 (2014).
[47] M.D. Johnson and C.R. Gwinn, Astrophys. J. **805**, 180 (2015).
[48] R.-S. Lu, F. Roelofs, V.L. Fish, et al., Astrophys. J., submitted.
[49] F. Eisenhauer, G. Perrin, W. Brandner, et al., The Messenger **143**, 16 (2011).